IPF coloring of crystal orientation data

R. Hielscher, G. Nolze

IPF coloring of crystal orientation data

G. Nolze[a]* and R. Hielscher [b]*

[a]Federal Institute for Materials Research and Testing (BAM), Unter den Eichen 87, 12205 Berlin, Germany, and [b]Technical University Chemnitz, Reichenhainer Str. 39, 09126 Chemnitz, Germany. Correspondence e-mail: gert.nolze@bam.de, ralf.hielscher@mathematik.tu-chemnitz.de

The inverse pole figure (IPF) coloring for a suitable evaluation of crystal orientation data is discussed. The major goal is a high correlation between encoding color and crystal orientation. Revised color distributions of the fundamental sectors are introduced which have the advantages of 1) being applicable for all point groups, 2) do not cause color discontinuities within grains, 3) featuring carefully balanced regions for red, cyan, blue, magenta, green and yellow, and 4) an enlarged grayish center in opposition to a tiny white center.

A new set of IPF color keys is proposed which is the result of an thorough analysis of the colorization problem. The discussion considers several topics: a) the majority of presently applied IPF color keys generates color discontinuities for specifically oriented grains, b) if a unique correlation between crystal direction and color is requested, discontinuity-preventing keys are possible for all point groups, except for $\bar{4}$, $\bar{3}$ and $\bar{1}$, c) for a specific symmetry group several IPF color keys are available visualizing different features of a microstructure, and d) for higher symmetries a simultaneous IPF mapping of two or three standard reference directions is insufficient for an unequivocal orientation assignment.

All color keys are available in MTEX, a free-available Matlab toolbox.

1. Introduction

For a spatially resolved characterization of crystalline materials orientation mapping performed, e.g., in a scanning electron microscope (SEM) by electron backscatter diffraction (EBSD) is a very efficient tool. This technique uses locally acquired Kikuchi patterns in order to assign the crystalline phase and derive the orientation **G** of the pattern-forming volume. Compilations of numerous applications derived over the years are given in (Schwartz *et al.*, 2000; Schwartz *et al.*, 2009).

Because of several hundred thousands of individual orientation measurements collected during a single microstructure mapping, one of the major challenges is a suitable visualization of such an enormous amount of orientation or misorientation data. A coloring of data is commonly used since it is impressed by a visually convinced encoding of a complex information. Therefore, in order to ensure the quantitative character of this imaging tool, appropriate color keys are required which shall enable an unequivocal, semi-quantitative and meaningful description of a crystal orientation by the encoding color.

Vicariously, the applied color key can be understood as the anisotropic distribution of any physical or chemical property of a crystalline phase. It indicates the variation of a property with changing crystal direction or orientation. Thus, an abrupt orientation change defines a grain or phase boundary and should preferably become visible by a remarkable color variation, at least for a crystal direction which is affected by the orientation change. Vice versa, sudden color changes are undesirable if no remarkable orientation changes occur. Since this is a general problem in color encoding of crystal orientation data, cf. e.g. Fig. 1, this was the major driving force of this work.

1.1. Coloring of Euler angles

A crystal orientation **G** is typically stored in terms of Euler angles, e.g., $\mathbf{G} = f(\varphi_1, \Phi, \varphi_2)$ following Bunge's notation (Bunge, 1982). It defines sequential rotations around three preselected reference axes, e.g., Z–X–Z, in order to bring a crystal from zero position into its orientation **G**. The easiest way for a mapping of orientation data is the encoding of the locally derived $(\varphi_1, \Phi, \varphi_2)$ by an assignment of each Euler angle to one of the primary colors Red (R), Green (G) and Blue (B), cf. Fig. 1 (a). The major disadvantage of this type of color encoding is the intricate interpretation of Euler angles, cf. e.g., (Bunge, 1982; Kocks *et al.*, 1998; Randle & Engler, 2000). The three angles are unevenly distributed with respect to the orientation description, e.g., already regarding the size of the angles itself. This affects their visualized orientation sensitivity which mainly concerns the evaluation of misorientations from Euler angles. However, most problematic is that regardless of the crystal symmetry Euler space encoding is affected by discontinuities in general, i.e., practically identical orientations can be encoded by clearly different colors. It represents the crucial reason that today's orientation maps are often only than colored by Euler angles if other options are missing or improperly implemented by the applied software package.

A typical case of color discontinuities within crystal orientation maps is represented in Fig. 1 (a) where the orientation-encoded color suddenly changes from violet to magenta within a single crystal. This happens since very similar orientations are defined by at least one totally different Euler angle, cf. the corresponding Φ-slice of the Euler space in Fig. 1 (b). Note that the comparatively big variations of φ_1 and φ_2 are only caused

research papers

by a small misorientation of maximal 2° within the displayed quartz grain[1]. The result is an occasional appearance of speckled and/or two-colored grains within the orientation map which restricts a doubtless interpretation of orientation measurements since such color jumps typically indicate systematic misindexing also, e.g., caused by any kind of pseudosymmetry, or an improper setup of the measuring system.

(a) Euler RGB

(b) Φ-section in Euler space

(c) IPF-Y map

(d) IPF key for $\bar{3}m$
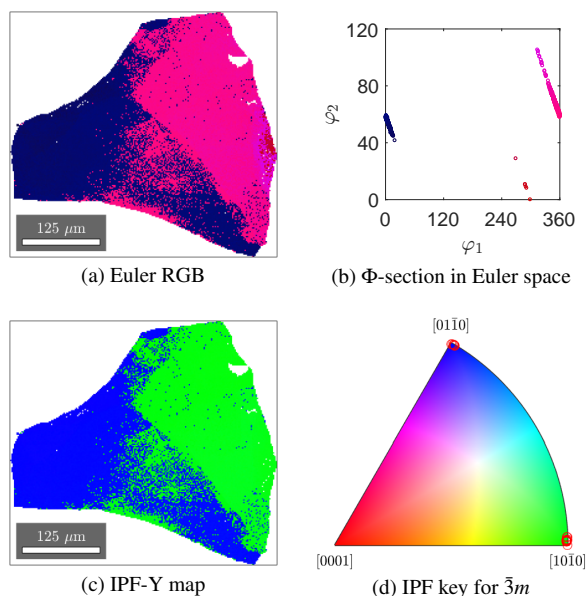
Figure 1
EBSD map of a single quartz grain. The color-discontinuities in the Euler map (a) are caused by the jump of the Euler angle φ_1 from 360° to 0° (b). The color distribution of the key for $\bar{3}m$ (d) displays the reason for the color jump visible in the IPF-Y map (c): the reference directions (red circles) close to the symmetry-equivalent $[1\,0\,\bar{1}\,0]$ and $[0\,1\,\bar{1}\,0]$ are displayed either in green or blue.

1.2. Ideal coloring

An ideal color encoding can be defined in a very pragmatic way. Any crystal orientation should be described by a color such that:

1. Similar orientations are associated with similar colors.

2. Different orientations are associated with different colors.

3. The difference in color of two orientations corresponds to the size of the misorientation angle.

4. The color definition is easily interpretable.

Unfortunately, it is mathematically impossible to construct a color encoding that satisfies at least the first two requirements. In other words, any color definition that unambiguously assigns colors to orientations will cause color jumps in orientation maps[2].

1.3. Potential and challenges of IPF coloring

In order to overcome this mere visualization problem of exaggerated color jumps in Euler maps, in 1987 another coloring has been introduced (Inokuti *et al.*, 1987). It is well-known as inverse pole figure (IPF) coloring and nowadays in vogue for the visualization of orientation data. The starting point is to fix a certain reference direction r as vector of the specimen coordinate system, e.g., r parallel to the sample surface normal (Z) or the tilt axis (X), and to describe it as direction h of the crystal lattice by taking the crystal orientation $\mathbf{G}$ into account:
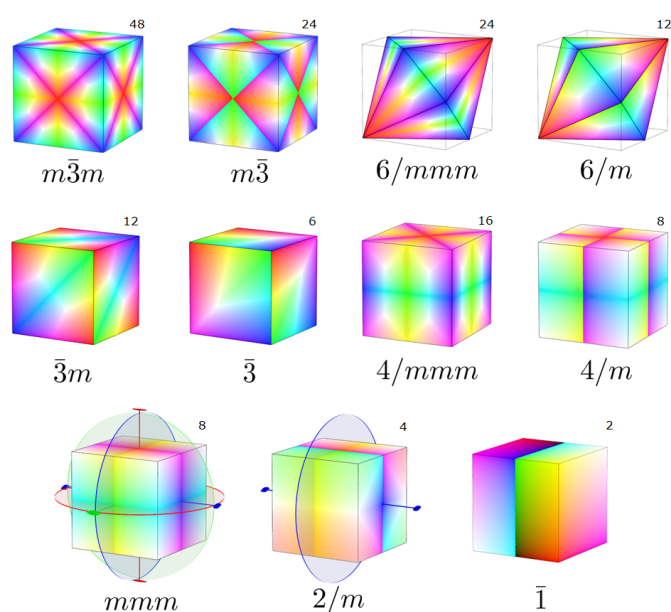
$$h = \mathbf{G}^{-1}r. \qquad (1)$$

This way each orientation $\mathbf{G}$ is assigned to some crystal direction h – its pole point in the r–inverse pole figure. Hence, by defining a colorization of the r–inverse pole figure one obtains a color definition for the orientation $\mathbf{G}$. In contrast to the coloring of Euler angles this assignment is not one-to-one as orientations that have the same crystal direction h parallel to r are depicted by the same color.

The set of all possible but crystallographically non-equivalent h defines the *fundamental sector* of a symmetry group $\mathcal{P}$. In combination with an asymmetric color distribution it represents the $\mathcal{P}$-specific IPF-color key. A presently in commercial software used color key for $\bar{3}m$ as Laue group symmetry of quartz ($\alpha-\mathrm{SiO}_2$) is exemplarily displayed in Fig. 1 (d).

By way of illustration, in Fig. 1 (c) the quartz grain is colored regarding the crystallographic description h of $r \parallel \mathrm{Y} = [0, 1, 0]$. The selection of $r \parallel \mathrm{Y}$ is responsible for the name of the map: IPF-Y. Unexpectedly, within the single quartz grain the encoding of h shows comparable color jumps as already displayed in the Euler angle map in Fig. 1 (a). In order to indicate the reason for this surprising result, in the colorized inverse pole figure, Fig. 1 (d), the pole positions of $h = \mathbf{G}^{-1}r$ are inserted as red circles. They expose that both symmetry-equivalent lattice directions $[1\,0\,\bar{1}\,0]$ and $[0\,1\,\bar{1}\,0]$ are misleadingly encoded by different colors.

Whether an IPF color key may cause color jumps in orientation maps or not becomes evident if the key is combined with the symmetry of the group, and plotted for all direction and not only for a single fundamental sector (Nolze, 2013). This is demonstrated in Fig. 2 for the 11 Laue groups considering IPF keys similarly used by the EBSD vendors. The color distributions projected on a surface of a cube or a hexagonal bipyramid visually prove that orientation maps free of color jumps may be guaranteed only for phases with the Laue-group symmetry $m\bar{3}m$, $6/mmm$, $4/mmm$, or mmm, i.e., only for 4 out of 11. Inspecting the crystal systems it is conspicuous that beside IPF maps of the still rarely investigated monoclinic and triclinic phases, obviously all maps can be affected by color jumps which visualize the IPF encoding of trigonal or rhombohedral phases (calcite, quartz, hematite etc.).

---

[1] The maximum misorientation angle of 2° has been refined by pattern matching of experimental and simulated Kikuchi patterns, cf. (Nolze *et al.*, 2016).
[2] Please note that for *misorientations* $\Delta\mathbf{G}_{AB} = \mathbf{G}_A\mathbf{G}_B^{-1}$ between two grains A and B a color encoding is possible that satisfy the first two requirements, cf. (Patala & Schuh, 2011; Patala *et al.*, 2012).

Figure 2
Standard color distribution combined with the 11 Laue groups. The projection onto the surface of a cube or a hexagonal bipyramid reflects color discontinuities for $m\bar{3}$, $6/m$, $\bar{3}m$, $\bar{3}$, $4/m$, $2/m$, and $\bar{1}$. The small numbers at the right-upper position give the multiplicities of the respective group.

1.4. Key topics of this paper

The IPF map in Fig. 1 (c) illustrates that even if size and shape of an IPF color key fulfill the requirements of a symmetry group, an improperly defined color distribution may generate physically meaningless discontinuities. Therefore, after some introductory remarks in Section 2 a generic approach for the generation of jump-free IPF color distributions is described which is applicable for the majority of point groups. Also the typically neglected different setup of crystallographic basis vectors are considered which are the result of an ambiguous alignment of symmetry elements, like $31m$ and $3m1$, or $\bar{4}2m$ and $\bar{4}m2$, cf. International Tables for Crystallography (Hahn, 1995), Table 10.1.2.2. Only for $\bar{1}$, $\bar{3}$, and $\bar{4}$ a simultaneously unequivocal and discontinuous-free assignment of colors is impossible so that in the present paper $\bar{1}$, $\bar{3}$, and $\bar{4}$ are excluded during discussion. Nevertheless, by way of illustration, for $\bar{1}$ a compromise is proposed which, however, does not enable an unequivocal assignment of a unique color to all h.

Given the fact that for the orientation determination common EBSD systems exclusively use the Laue-group symmetry of a phase, it might surprise that we suggest an introduction of IPF keys for all 32 point groups. This has several reasons. On the one hand, we will show that even in case of a centrosymmetric phase the IPF coloring enhances the discriminability of differently oriented crystals by consideration of the symmetry of the respectively 11 maximal enantiomorphic subgroup. On the other hand, it is well-accepted that EBSD is not *a priori* a centrosymmetric technique (Baba-Kishi, 1991; Winkelmann & Nolze, 2015a; Nolze *et al.*, 2015) so that any limitation on Laue

groups and their enantiomorphic subgroups is obsolete, and an adaptation of the respective imaging tools is required.

For good measure, in Section 3.1 we disprove the common belief that two or three IPF maps are sufficient for an unequivocal orientation identification. Exemplarily, we illustrate this by the identical coloring of non-equivalent transformation variants of $\gamma-$Fe precipitates. However, it is meant as a very exclusive subset of a general orientation measurement.

All IPF keys are implemented in the free-available Matlab toolbox MTEX-4.3 (Bachmann *et al.*, 2010). The equal-area projections of the entire color distributions for all $\mathcal{P}$ are listed in Appendix B. All illustrations presented in this paper have been generated exclusively by MTEX-4.3. The corresponding documented script files are publicly available at http://mtex-toolbox.github.io/publications.html.

2. Advanced color keys for IPF color coding

The clear color jumps within the orientation map of a single quartz grain in Fig. 1 were the most annoying features and origin of this review. Therefore, this section has the aim to generate color distributions which guarantee a discontinuous-free IPF encoding of similar orientations. According to Section 1.4, we do not restrict ourselves to Laue groups but consider all 32 point groups inclusive well-accepted deviations in basis vector definitions.

2.1. Some general remarks

As postulated by equ. (1), a general orientation is uniquely defined by a matrix $\mathbf{G}$ which maps the Cartesian reference coordinate system onto a Cartesian description of the crystal coordinate system, or vice versa (passive or active rotation, see e.g., (Nolze, 2015)). Despite describing the same orientation, the derived $\mathbf{G}$ might look diverse and therefore described by different triples of Euler angles. This is caused by the unambiguous definition of crystallographic basis vectors as consequence of the phase-inherent crystal symmetry.

2.1.1. Symmetry-specific orientation description Using $\mathbf{W}_{\mathcal{P}}$ as symbol for a symmetry operator of the point group $\mathcal{P}$, an EBSD software may return any of the orientations $\mathbf{GW}_{\mathcal{P}}$ as possible indexing solution. The only restriction is that $\mathbf{W}_{\mathcal{P}}$ has to be a proper rotation $\mathbf{W}_{\mathcal{P}}^{+}$ with $\det \mathbf{W}_{\mathcal{P}}^{+} = 1$, since only they do not turn the describing right-handed into a left-handed coordinate system. Therefore, orientation-equivalent directions to $h = \mathbf{G}^{-1}r$ are actually given by

$$(\mathbf{GW}_{\mathcal{P}}^{+})^{-1}r = (\mathbf{W}_{\mathcal{P}}^{+})^{-1}\mathbf{G}^{-1}r = (\mathbf{W}_{\mathcal{P}}^{+})^{-1}h. \quad (2)$$

From this follows that even for centrosymmetric groups one can distinguish between h and $-h$. It also explains why for a phase with symmetry $m\bar{3}m$ in exemplarily contributions like (Kocks *et al.*, 1998; Randle & Engler, 2000; Nolze, 2015) only 24 equivalent orientations are listed and not 48 as defined by the order of $\mathcal{P} = m\bar{3}m$.

It is particularly advantageous that the subset of all $\mathbf{W}_{\mathcal{P}}^{+}$ defines the maximal enantiomorphic subgroup $\mathcal{H}_{\mathcal{P}}$ of $\mathcal{P}$, so that

for any point group $\mathcal{P}$ a well-defined relationship for an orientation description exists. Thus one can conclude that for any non-enantiomorphic $\mathcal{P}$ the maximal enantiomorphic subgroup $\mathcal{H}_{\mathcal{P}}$ is used for the orientation description.

2.1.2. Laue-group addiction Even if a not-centrosymmetric phase is investigated, up to now EBSD systems are not yet designed to discriminate the signal with respect to $\mathcal{P}$ but to the corresponding Laue group $\mathcal{S}$ only. This has its origin in the experimental observation that for the majority of phases deviations from a centrosymmetric diffraction signal are negligibly small (Friedel's rule).

By using the higher symmetric Laue group $\mathcal{S}$, the symmetry operations $\mathbf{W}_{\mathcal{S}}^{+} \in \mathcal{H}_{\mathcal{S}}$ of the maximal enantiomorphic subgroup $\mathcal{H}_{\mathcal{S}}$ of $\mathcal{S}$ are considered for *orientation* description. Hence, the following crystal directions has to be considered as equivalent

$$(\boldsymbol{W}_{\mathcal{S}}^{+})^{-1}h = (\boldsymbol{W}_{\mathcal{S}}^{+})^{-1}\mathbf{G}^{-1}r. \tag{3}$$

Please note that the maximal enantiomorphic subgroup $\mathcal{H}_{\mathcal{S}}$ of the Laue group $\mathcal{S}$ in general does not coincide with the point group $\mathcal{P}$ nor with its maximal enantiomorphic subgroup $\mathcal{H}_{\mathcal{P}}$.

Depending wether $\mathcal{P}$ is enantiomorphic the multiplicity of $\mathcal{H}_{\mathcal{S}}$ is either the same or twice the multiplicity of $\mathcal{H}_{\mathcal{P}}$. The size of the fundamental sector of $\mathcal{H}_{\mathcal{S}}$ is either the same or half the size of the fundamental sector of $\mathcal{H}_{\mathcal{P}}$.

However, the hitherto used IPF-coloring is exclusively related to the Laue group $\mathcal{S}$ of $\mathcal{P}$, i.e., the derived IPF maps always assign the *same* color for regarding $\mathcal{P}$ non-equivalent directions h and $-h$:

$$(\boldsymbol{W}_{\mathcal{S}})^{-1}h = (\boldsymbol{W}_{\mathcal{S}})^{-1}\mathbf{G}^{-1}r, \quad \boldsymbol{W}_{\mathcal{S}} \in \mathcal{S}. \tag{4}$$

2.1.3. Meaningful selections and suitable coloring For a definition of an IPF-color key the restriction to the fundamental sector of the symmetry group is beneficial, since it enables the encoding of symmetry-equivalent h by the same color. In order to prevent different colors for practically symmetry-equivalent h one only has to ensure the use of a suitable color distribution for the respective fundamental sector of $\mathcal{P}$. Here beside the asymmetry of the color distribution an additional condition is important. Two orientations $\mathbf{G}_1$ and $\mathbf{G}_2$ should become encoded by a similar color if their misorientation $\Delta\mathbf{G}_{1,2} = \mathbf{G}_1\mathbf{G}_2^{-1}$ is very small. This is what went wrong in the introductory example, since the by red circles in Fig. 1 (d) illustrated h are close to the symmetry-equivalent $[10\bar{1}0]$ (green) and $[01\bar{1}0]$ (blue).

2.2. No symmetry: $\mathcal{P} = 1$

In case of no symmetry the fundamental sector is defined by all possible h and described by the entire projection sphere. Each point on the sphere is given by its polar coordinates (θ, ρ) where the polar angle θ runs on the upper hemisphere from $0 \ldots 90°$ and on the lower hemisphere from $90 \ldots 180°$; and the azimuth angle ρ runs from $0 \ldots 360°$. In order to define an asymmetric color distribution for the entire sphere we describe the color by the three values hue H, saturation S and lightning L, and set $H = \rho$, $S = 1$ and $L = \theta$, cf. Fig. 3. Note that we are

quite flexible in distributing the colors on the sphere. Some additional adaptions that lead to more balanced color distributions are discussed in Appendix A.
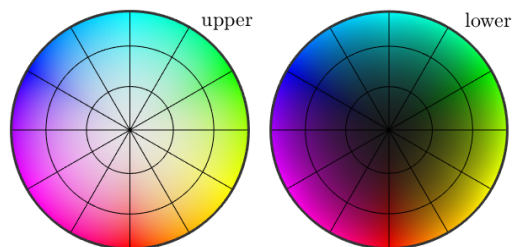
Figure 3
Colorization of the unit sphere (right: upper half, left: lower half) using fully saturated colors, i.e., $S = 1$ with hue H being the azimuth of a point on the sphere and the lightning L being the polar angle.

In the subsequent sections the color keys for all other crystal symmetries are defined by transforming the corresponding fundamental sectors in a suitable way onto the sphere and making use of the colorization we just discussed.

2.3. Mirror symmetry: $\mathcal{P} = m$

In case of a single mirror symmetry m ($\equiv \bar{2}$) the fundamental sector is reduced to a hemisphere. After mirroring any color distribution of the fundamental sector onto the opposite hemisphere, along the transition line between both hemispheres no color discontinuities occur. Thus, the color distribution given for the upper hemisphere in Fig. 3 is a suitable discontinuity-free color key for point group m.

An interesting question is, whether it is possible to define a color key for point group m that contains not only all the bright colors from the upper hemisphere of Fig. 3 but also all the dark colors from the lower hemisphere. As a matter of fact it can be proven that this is impossible.

2.4. Standard color keys

The fundamental sector of a point group with order k higher than 2 can be chosen either as a spherical lune, triangle, or square. In order to colorize these different shapes they are transformed onto the upper hemisphere such that the barycenter p of the sector is rotated into the North Pole. For any point inside the sector the polar angle is defined as the distance to the barycenter p which is scaled in a way that the boundary of the sector has a polar angle of $90°$, i.e., it is transformed onto the equator. The azimuth is given by the angle to the barycenter relatively to some fixed vertex of the sector. The color of any h inside a fundamental sector is determined as description of the hue H by the azimuthal angle ρ, and of the lightning L by the polar angle θ of h, cf. Section 2.2. For illustration this is sketched in Fig. 4 (a), (b) and (c). Some more technical details about this mapping procedure are given in Appendix A.

We will refer to a color key generated as described in this section as key with a *standard* color distribution, or as *standard color key*. Note, that a standard color key either contains a dark or a bright center. Contrary, the color key for the point group 1

as defined in Section 2.2 contains both a bright and a dark center. Therefore, we will refer to it as key with an *extended* color distribution, or describe it shortly as *extended color key*.

(a) *mmm*

(b) *m3̄m*

(c) *3m*
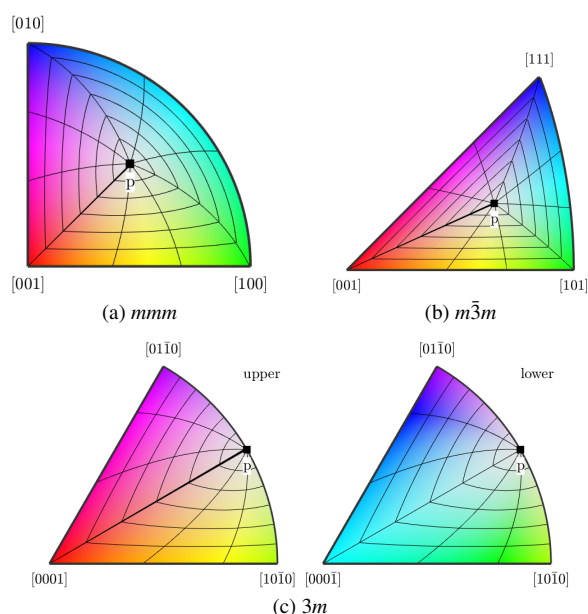
Figure 4
The fundamental sectors for orthorhombic symmetry (a), cubic symmetry *m3̄m* (b), and trigonal symmetry *3m* (c). For illustration, the barycenter *p*, grid lines for the polar angle at 15°, 30°, 45°...90°, and grid lines for the azimuth angle at 0°, 40°, 80°...360° are overlaid. Because of symmetry, the color range only uses the half of the general color range displayed in Fig. 3. The color distribution of a hemisphere is transformed onto the spherical triangle by using the polar coordinates.

2.5. Fundamental sectors with reflection boundaries

As visible in Fig. 2, the standard color distribution is applicable for some Laue groups only. In fact the following result holds true: The fundamental sector of a point group can be colorized by the standard color distribution without discontinuities at the boundary of the fundamental sector if and only if all the boundaries are crystallographic mirror planes. The point groups which fulfill this condition are listed in Table 1 in the column "standard". Thus, the standard color distribution is applicable for all polar and non-enantiomorphic (green), but also some centrosymmetric (black) and non-centrosymmetric (blue) groups.

A more systematic analysis of the crystallographic symmetry shows that, if one describes R (R ∈ W$^+$) as *main* rotation axis[3], all groups with mirror planes $\bar{2} \perp R$ have to use the standard color distribution. Moreover, all groups containing additional two-fold rotation axes fulfilling the conditions a) $2 \perp R$ and b) $2 \perp \bar{2}$ are uniquely described by the standard color distribution as well. Examples are $\bar{6}2m$ or $\bar{4}3m$, but not $\bar{4}2m$, as shown in Table 1. All remaining symmetry groups – except $\bar{1}$, $\bar{3}$ and $\bar{4}$ – are uniquely defined by the extended color distribution as it will be shown in Section 2.6. Table 1 sorts the groups with respect to the order *k*, i.e., all groups with the same order have the identical size (but not shape) of the fundamental sector, e.g. 422, $\bar{4}2m$

---

[3] For the cubic system the main rotation axes R are 3 or $\bar{3}$ parallel ⟨1 1 1⟩.

and 4/*m*, but also 4*mm* and *mmm*. For a certain group $\mathcal{P}$ a maximal subgroup relationship of index [2] is given by the groups behind (horizontal) and below (vertical) with the half size of *k*. Index [*i*] defines the ratio between the orders for group and subgroup. Transitions between point groups of different lattices are not straightforward so that only relationships within a lattice are easily recognizable. For example, maximal subgroups of 6/*mmm* are $\bar{6}2m$ and 6*mm*, but also 622, $\bar{3}m$ and 6/*m*. For 32 the only subgroup of index [2] is 3.

Table 1
Point groups differentiated by the type of the translation lattice, and whether they enable a discontinuous-free imaging by standard or an extended color distribution. By color we distinguish among **centrosymmetric** (Laue), non-centrosymmetric, polar, enantiomorphic, and polar + enantiomorphic groups. For $\bar{3}$, $\bar{4}$ and $\bar{1}$ neither the standard nor the extended color distribution is suitable. *k* defines the order of the respective groups.

lattice type	k	standard	k		extended			no
cubic	48	*m3̄m*	24	432	*m3̄*			
	24	$\bar{4}3m$	12		23			
hexagonal	24	**6/mmm**	12	622	$\bar{3}m$	6/*m*		
	12	$\bar{6}2m$	6		32		$\bar{6}$	$\bar{3}$
	12	6*mm*	6			6		
	6	3*m*	3				3	
tetragonal	16	**4/mmm**	8	422	$\bar{4}2m$	4/*m*		$\bar{4}$
	8	4*mm*	4			4		
orthorhombic /	8	***mmm***	4		222	2/*m*		$\bar{1}$
monoclinic /	4	*mm*2	2			2		
triclinic	2	*m*	1				1	

2.6. Extended color keys

Fig. 2 showed, that for 7 Laue groups the application of the standard color distribution to a fundamental sector which is not entirely bounded by mirror planes leads to color discontinuities. This is again illustrated in Fig. 5 (a) as equal area projection for $\mathcal{P} = m\bar{3}$. Smooth color transitions through the reflection boundaries ‖ {1 0 0} occur, but along {1 1 0} partially color discontinuities are detectable.

(a)   (b)   (c) extended
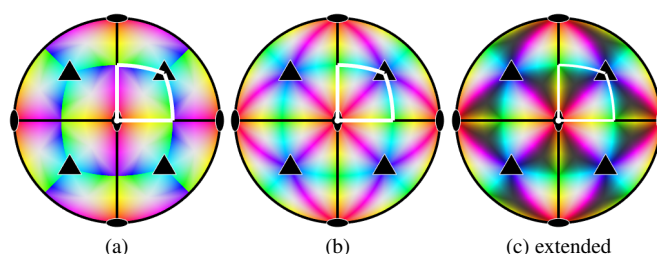
Figure 5
Different color distributions applied on the fundamental sector (white-framed) of $\mathcal{P} = m\bar{3}$. The standard color distribution in (a) is defined according to Section 2.4. The color distribution in (b) corresponds to super group $m\bar{3}m$ and suffers from ambiguity. The color distribution in (c) is free of discontinuities and unambiguously assigns a single color to all symmetry-equivalent *h*.

research papers

A simple way to overcome these color discontinuities is to consider a definition that is not only invariant with respect to the point group $\mathcal{P}$ but with respect to some super group $\mathcal{P}_+$ which is chosen such that its fundamental sector is entirely bounded by mirroring planes. In Table 1 for any point group $\mathcal{P}$ the minimal supergroup $\mathcal{P}_+$ with this property is listed in the same row in the column "standard". For $\mathcal{P} = m\bar{3}$ the matching super group is $m\bar{3}m$. The corresponding key in Fig. 5(b) is free of color discontinuities but ambiguous in the sense that symmetrically non-equivalent directions are associated with the same color.

For all point groups $\mathcal{P}$ listed in the column "extended" of Table 1 the multiplicity is exactly twice the multiplicity of the matching super group $\mathcal{P}_+$ in the column "standard". Accordingly, the fundamental sector of $\mathcal{P}_+$ is half the size of the fundamental sector of $\mathcal{P}$. This allows us to colorize the half of the fundamental sector of $\mathcal{P}$ which coincides with the fundamental sector of $\mathcal{P}_+$ with a bright center using the barycentric coordinates to assign a color from the upper hemisphere, cf. Section 2.4. The remaining half will be colorized with a dark center, i.e., by using barycentric coordinates to assign a color from the lower hemisphere. The resulting key does not generate any color discontinuities since along the boundaries of the fundamental sectors the impact of the bright as well as of the dark center is zero and the colors along this connection zone are identical. For $m\bar{3}$ the so derived key is displayed in Fig. 5(c). Following this approach one can define unambiguous and discontinuity-free keys for all point groups listed in the column "extended" of Table 1.

The general procedure for encoding an orientation **G** by an extended color distribution is described as follows:

1. Compute the crystal direction $h = \mathbf{G}^{-1}r$.

2. Transform h into the fundamental sector of point group $\mathcal{P}$, i.e., find a symmetry operation $W \in \mathcal{P}$, so that Wh is inside the fundamental sector.

3. Project h into the fundamental sector of the super group $\mathcal{P}_+$, i.e., find a symmetry operation $W_+ \in \mathcal{P}_+$, such that W_+h is inside the fundamental sector.

4. Determine the coordinates (θ, ρ) of the barycenter for W_+h according to Section 2.4.

5. Check whether W_+h and Wh coincide. If this is not the case, mirror (θ, ρ) to the lower hemisphere, i.e., replace θ by $(\pi - \theta)$.

6. Apply the triclinic IPF key as defined in Section 2.2 to assign a color to (θ, ρ).

2.7. The exceptional groups $\bar{1}$, $\bar{3}$, and $\bar{4}$

The fundamental sectors of these groups are topologically equivalent to the so-called two-dimensional projective space. It can be mathematically proven that there is no jump-free embedding of these sectors into the three-dimensional space (Massey, 1959). In consequence, for $\bar{1}$, $\bar{3}$, and $\bar{4}$ any IPF distribution will either cause color jumps, or assign the same color to crystallographically non-equivalent directions. For point group $\bar{1}$ both possibilities are compared in Fig. 6. For the standard

color distribution in (a) color jumps are generated along the entire equatorial line when moving from the upper to the lower hemisphere. An alternative color distribution in (b) prevents any color jump but assigns the same color (black) to all h defining the equatorial line.

(a) unambiguous IPF key for $\bar{1}$

(b) jump free IPF key for $\bar{1}$
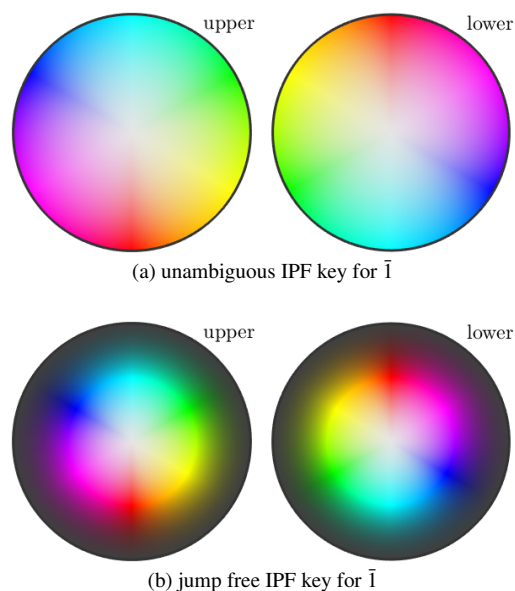
Figure 6
Two IPF keys for Laue group -1. An ambiguity free IPF key with color jumps at the equator (a) and a color jump free IPF key with ambiguous directions around the equator (b).

(a) unambiguous IPF key for $\bar{3}$

(b) unambiguous IPF key for $\bar{4}$
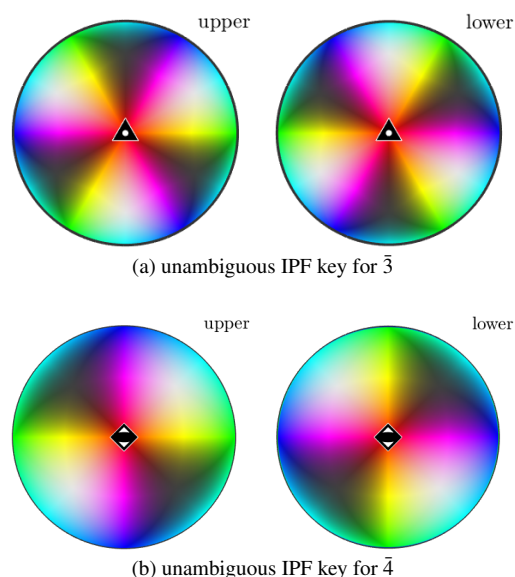
Figure 7
IPF keys for the Laue group $\bar{3}$ (a) and the non-centrosymmetric group $\bar{4}$ (b) with color jumps at the equator, i.e., at the same position on the circumference for the upper as well as for the lower hemisphere the same color should exist. Instead an abrupt change from green to blue is visible.

For illustration, in Fig. 7 the symmetries of $\bar{3}$ and $\bar{4}$ are combined with the extended color distributions. Along the equatorial line upper and lower hemisphere always reflect a transition

from blue to green. Only for the directions exactly between blue and green the same color (turquoise) is identical for both hemispheres.

3. Applications

In the following we will discuss the advantages of the IPF coloring considering different symmetries, i.e., we will answer the question, which symmetry should be selected for which kind of orientation data visualization. First, an example will illustrate the limited uniqueness of the currently used IPF coloring.

3.1. On the uniqueness of IPF color encoding

Since an unequivocal interpretation of a crystal orientation $\mathbf{G}$ by only one reference direction r is impossible, usually several IPF maps are combined. However, it is common but unfortunately wrong to believe that with two or three IPF maps for X, Y and Z all orientations are uniquely color-encoded. This is only true for the triclinic case. The reason is that for two reference directions r_1, r_2 and two crystal direction h_1, h_2 the fiber of orientations $\mathbf{G}$ with $\mathbf{G}h_1 = r_1$ and the fiber of orientation $\tilde{\mathbf{G}}$ with $\tilde{\mathbf{G}}h_2 = r_2$ intersects for triclinic symmetry in at most one orientation. For higher symmetries, however, also intersections between crystallographically equivalent fibers may occur.

The most basic counter example appears for the monoclinic point group $\mathcal{P} = 121$ and the symmetrically not equivalent orientations $\mathbf{G}_1 = (0°, 0°, 0°)$ and $\mathbf{G}_2 = (180°, 0°, 0°)$. Both orientations have the same poles (001) and $(00\bar{1})$ in the Z–inverse pole figure and the same poles (100) and $(\bar{1}00)$ in the X–inverse pole figure. Therefore, both orientations would be colored identically in the IPF-Z map as well as in the IPF-X map.

For a more practical illustration we selected the highest cubic crystal symmetry. In Fig. 8 the 24 orientation variants of $\gamma-$Fe are displayed which are formed during transformation of a single grain of $\alpha-$Fe according the Kurdjumov-Sachs model. The small maps of 6×4 squares depict each orientation variant. The lines between the squares indicate the grain boundaries (maximal misorientation angle: 5°). Although the orientations of all variants are undoubtedly different, the existence of only 3 points within the inverse pole figure in Fig. 8 (e) instead of the expected 24 verifies that several variants are described by the same h. In consequence, within the pole figure only three colors appear: red and two slightly different greens. Focusing on the red-colored variants in the IPF-Y map (middle), four of them are also identically colorized in IPF-X and IPF-Z, i.e., at least these variants cannot be distinguished. In order to recognize the related poles within the pole figure, they are there labeled as well.

It becomes clear that with respect to the standard reference directions X, Y, and Z the $\{100\}$ poles appear rotation-symmetric to each other. Applying the rotation symmetry ∥Z, variant 1 and 2, as well as variant 3 and 4 meet in the same pole positions.

(a) IPF-X map   (b) IPF-Y map   (c) IPF-Z map

(d) (100) pole figure   (e) IPF color key
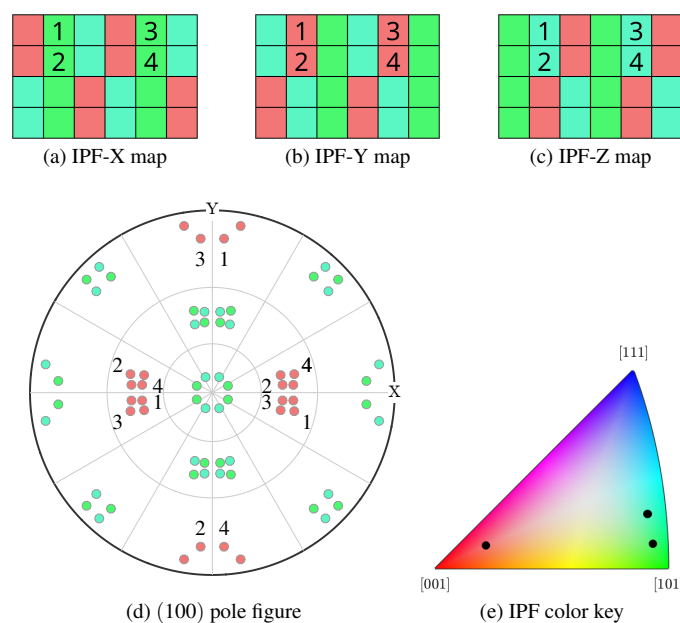
Figure 8
The 24 variants of the Kurdjumov–Sachs orientation relationship. The orientation variants are encoded for r_x (a), r_y (b), and r_z (c). The poles in the (100) pole figure (d) are colorized according to the coloring of r_y. The IPF color key in (e) shows only three instead of the expected 24 pole positions for h which proves that orientations of different variants are encoded by the same color and cannot be distinguished.

(a) IPF-X map   (b) IPF-Y map   (c) IPF-Z map

(d) (100) pole figure   (e) IPF color key
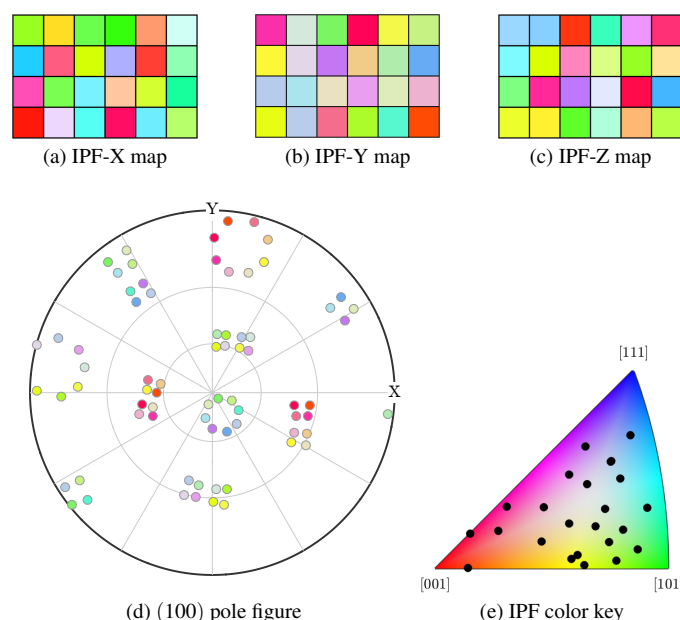
Figure 9
The 24 orientation variants of $\alpha-$Fe (Kurdjumov–Sachs orientation relationship) assuming a general alignment of the parent $\gamma-$Fe grain. All colorized maps (a-c) as well as the (100) pole figure (d) and inverse pole figure for reference direction $r \parallel$ Y (e) represent all variants by different colors.

For comparison, in Fig. 9 a slightly rotated pole distribution is represented where the variants are no more symmetrically

aligned to X, Y and Z. As expected for general orientations, already within the inverse pole figure 24 different h appear, and therefore the poles of all variants within the pole figure have different colors and can be clearly distinguished.

3.2. Laue versus point versus enantiomorphic group

As already theoretically sketched in Section 2.1, orientation data derived from Kikuchi patterns are until today per default related to the Laue group $\mathcal{S}$ of the investigated phase. However, it can be beneficial to colorize orientation data with respect to the maximal enantiomorphic subgroup $\mathcal{H}_\mathcal{P}$ of the point group, or $\mathcal{H}_\mathcal{S}$ of the Laue group.

Therefore, for a systematic discussion of an IPF coloring three different cases can be distinguished:

1. the point group $\mathcal{P}$ is centrosymmetric, i.e., it is a Laue group,

2. the point group $\mathcal{P}$ is enantiomorphic, i.e., $\mathcal{P}$ only contains proper rotations, and

3. the point group $\mathcal{P}$ is neither a centrosymmetric nor an enantiomorphic group.

3.2.1. Encoding for centrosymmetric point groups. If the point group $\mathcal{P}$ is centrosymmetric the common assumption of an automatic substitution of $\mathcal{P}$ by its Laue group is redundant. A coloring of h according to $\mathcal{P}$ is then absolutely permissible since no improper simplifications have been applied. The limitations of this orientation coloring has been already illustrated by the example of the transformation variants given in Section 3.1. In case of a very symmetric orientation of the parent $\alpha-$Fe grain, four variants cannot be distinguished using the color-key $\mathcal{P} = m\bar{3}m$, cf. Fig. 8.

On the other hand, according to the explanations briefly given in Section 2.1 the orientation of a centrosymmetric group is defined by $W_\mathcal{P}^+$ describing the maximal enantiomorphic subgroup $\mathcal{H}_\mathcal{P}$. Therefore, for a maximal orientation visualization the color key of $\mathcal{H}_\mathcal{P}$ is most helpful. Since this key practically differs between h and $-h$, it enhances the discriminability of crystal orientations.

This can be nicely illustrated by comparing the impact of the color key of $\mathcal{P} = m\bar{3}m$ in Fig. 8 with the color key of $\mathcal{H}_\mathcal{P} = 432$ in Fig. 10. Using $\mathcal{H}_\mathcal{P}$, already the IPF maps of two standard reference directions suffice a discrimination of all 24 variants. For the same symmetric alignment the inverse pole figure in Fig. 10 (d) contains again all 24 variants, but the consideration of the enantiomorphic symmetry encodes them by already six different colors, which explains the higher discriminability.

Summarizing the IPF coloring of a centrosymmetric phase one can state that there are two possible but non-equivalent opportunities:

a) coloring with respect to $\mathcal{P}$, and

b) coloring with respect to $\mathcal{H}_\mathcal{P}$.

The first is preferred for a simple coloring of a reference direction r in order to display any correlation of a parallel-aligned loading axis, rolling or growing direction, temperature or concentration gradient, etc. to one or more crystallographic directions h. The orientation is here only tool to determine all symmetry-equivalent h of $\mathcal{P}$. If a real visualization of the orientation is required, the better choice is the use of (b), since there any kind of symmetrization of orientation data is excluded.


(a) IPF-X map   (b) IPF-Y map   (c) IPF-Z map

(d) (100) pole figure   (d) IPF color key for 432
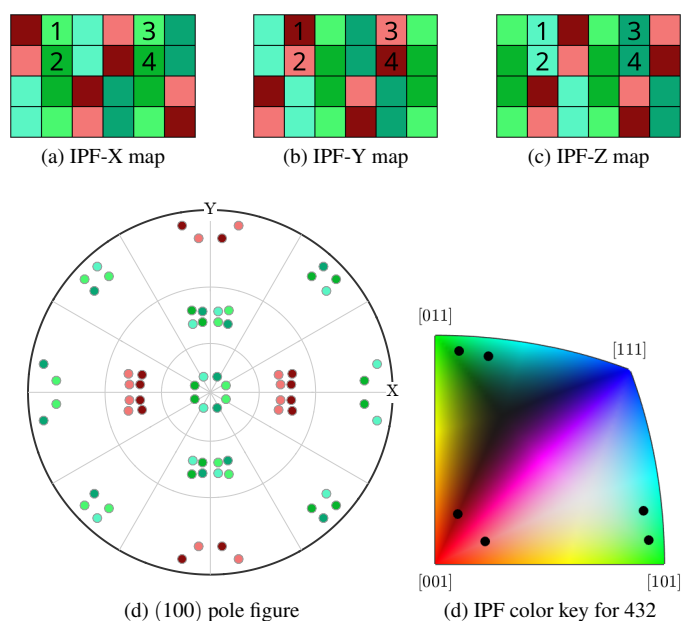
Figure 10
IPF maps for (a), Y (b), and Z (c) displaying the 24 variants of the Kurdjumov–Sachs orientation relationship in the same alignment as given in Fig. 8. In (d) the color key for the enantiomorphic point group 432 is shown. The black dots define the six possible crystallographic descriptions of either X, Y, or Z.

3.2.2. Encoding for enantiomorphic point groups. In this case, the native symmetry of the considered phase contains only proper rotations. Although all presently existing commercial EBSD systems use the Laue group $\mathcal{S}$ for the indexing of Kikuchi patterns, the derived orientation description is always related to the maximal enantiomorphic subgroup $\mathcal{H}_\mathcal{S}$, cf. Section 3.2.1. Since here $\mathcal{P} = \mathcal{H}_\mathcal{S}$, two color encodings are available: with respect to $\mathcal{P}$ and with respect to $\mathcal{S}$.

To illustrate the difference between them we re-examine the introductory example of quartz which is described by the enantiomorphic point group 321 but indexed according to $\bar{3}m1$. The centrosymmetric key for $\bar{3}m1$ is displayed in Fig. 11 (a), whereas (c) shows the resulting entire color distribution after application of the symmetry on the color key.

Note that this key generated according to Section 2 is different from the one used in Fig. 1. The key of the enantiomorphic group 321 is displayed in Fig. 11 (b). As result of the halved order k caused by the maximal subgroup relationship, the size is twice that big compared to (a). (d) shows again the color distribution after application of the point group symmetry. Both entire color distributions in Fig. 11 (c) and (d) verify the discontinuous-free character of the newly defined color keys.

(a) $\bar{3}m1$

(b) 321, i.e., $\parallel \langle 1\,1\,\bar{2}\,0\rangle$

(c) $\bar{3}m1$, full color distribution
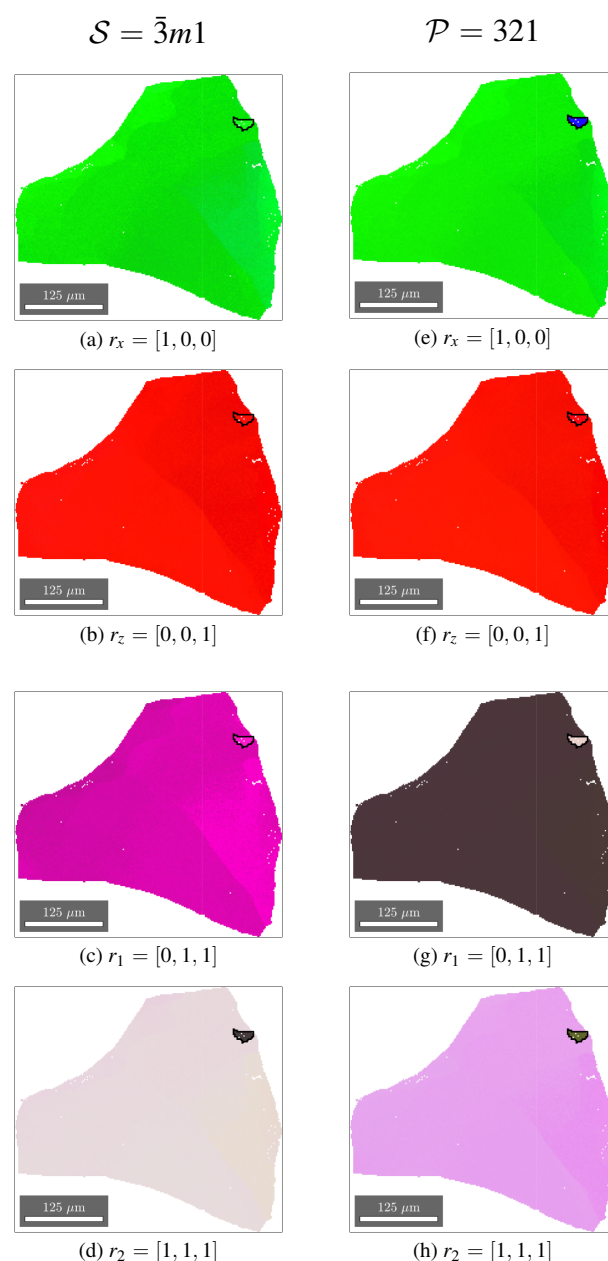
(d) 321, full color distribution
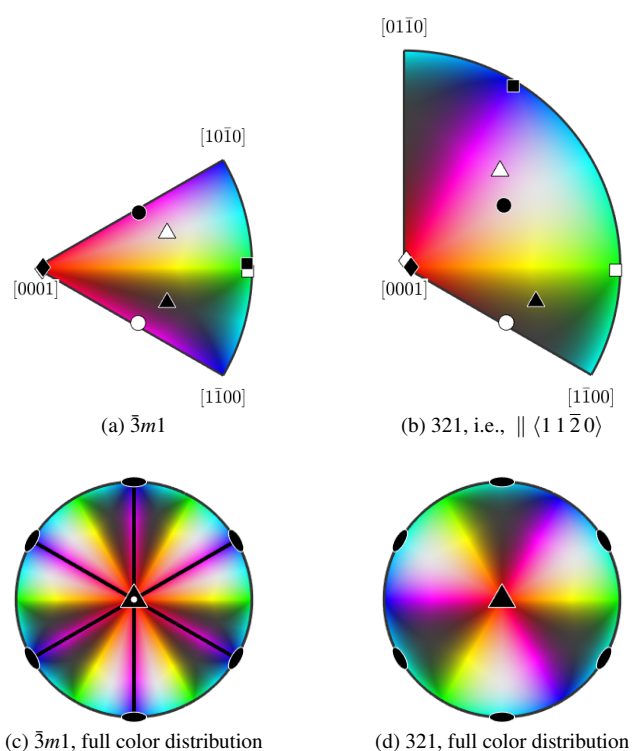
Figure 11
IPF keys for the fundamental sectors of the Laue group $\bar{3}m1$ (a) and its maximal enantiomorphic subgroup 321 (b). The poles corresponding to the directions r_x ($\square$), r_z ($\diamond$), r_1 ($\circ$) and r_2 ($\triangle$) are colored black for the host grain and white for the twinned inclusion. In (c) and (d) the equal-area projections of the entire color distributions are given overlaid by the symmetry elements of the respective groups.

$\mathcal{S} = \bar{3}m1$ $\mathcal{P} = 321$

(a) $r_x = [1, 0, 0]$ (e) $r_x = [1, 0, 0]$

(b) $r_z = [0, 0, 1]$ (f) $r_z = [0, 0, 1]$

(c) $r_1 = [0, 1, 1]$ (g) $r_1 = [0, 1, 1]$

(d) $r_2 = [1, 1, 1]$ (h) $r_2 = [1, 1, 1]$

Figure 12
The quartz grain from Fig. 1 colorized by the adapted IPF key of $\mathcal{S}$ (left), and by the IPF key of $\mathcal{P}$ (right). The used color keys are given in Fig. 11. The different maps color-coding different reference directions. A small twin is marked by a black boundary.

The most interesting question is, how the different symmetries for the orientation description of quartz will affect the finally derived IPF maps? To this end, in Fig. 12 the IPF maps generated for different reference directions are compared according to the Laue group $\mathcal{S} = \bar{3}m1$ (left column) and the originally enantiomorphic point group $\mathcal{P} = 321$ (right column). As expected from Fig. 11 (c) and (d), both applied color keys successfully avoid the color jumps generated by a today still used standard color key in Fig. 1. However, caused by the different color definition for $\mathcal{S}$ and $\mathcal{P}$, IPF maps of both symmetries only appear similar for specific crystal orientations.

We would like to focus the attention of the readers to the little twin outlined by its black grain boundary at the top right in the IPF map. Caused by a Brazil or Dauphiné law, the twin is surprisingly often encoded by almost the same colors as the host crystal. With respect to the color encoding of $\bar{3}m1$, the IPF maps of r_x, r_z and $r_1 = [0, 1, 1]$ are concerned, and only for a general reference direction $r_2 = [1, 1, 1]$ host and twin orientation can be visually distinguished.

In contrast, by the use of the color key of 321 only the accidental alignment of $r_z \parallel [0\,0\,0\,1]$ which is either twin axis or part of the twin plane leads to similar colors for host and twin. For all other reference directions host and twin orientation are clearly discriminable.

A detailed observation of $h = \mathbf{G}^{-1}r$ projected in the IPF in Fig. 11 can explain this phenomenon more clearly. First, we are concentrating on the IPF of $\bar{3}m1$ (a). The applied reference directions are described by different symbols: r_x ($\square$), r_z ($\diamond$), $r_1 = [0, 1, 1]$ ($\circ$), and $r_2 = [1, 1, 1]$ ($\triangle$). The presentation shows that host (black symbols) and twin orientation (white symbols) are therefore encoded by nearly the same color since their poles are given by practically identical directions h_x, h_z, h_1, and h_2. The reason is that for some of the chosen reference directions the symmetry along the circumference of the IPF key accidentally fits to the symmetry of the Brazil and Dauphinè

law. In general: if a reference direction *r* is close to the peripheral zones of the fundamental sector, host grain as well as twin will be colorized by the same color, because of the newly introduced symmetry property of the color distribution along the periphery. Only if a reference direction occupies a general direction *h* — △ — a different color encoding of both host and twin orientations is also possible for a Laue-group related coloring, cf. Fig. 12 (d). Since in a polycrystalline material practically any orientation can appear, a certain probability exists that reference directions of differently orientated grains are aligned along or close to the peripheral zone of the fundamental sector and cannot be distinguished by their color anymore. Differently oriented grains become identically colored.

As comparison, the positions of *h* in Fig. 11 (b) are no more mirror-symmetrically aligned with respect to $\{1\bar{1}00\}$. Using the color key of the enantiomorphic group one can now also visually distinguish between both twinned grain by their different color, cf. Fig. 12 (e, g-h). The only exception is the IPF-Z map, where r_z is arbitrarily parallel to $[0\,0\,0\,1]$ and therefore host and twin are both red-colored, cf. Fig. 12 (f).

Summarizing this case, phases with enantiomorphic symmetry can be either color-coded by their enantiomorphic symmetry, if this symmetry is recognizable. However, if the orientation description is based on the respective Laue group $\mathcal{S}$ the application of the enantiomorphic group $\mathcal{H}_\mathcal{S} = \mathcal{P}$ can be beneficial as demonstrated at the twin of quartz, or also for the previous example of the transformation variants of $\gamma-$Fe. However, it needs to be pointed out that despite $\mathcal{H}_\mathcal{S} = \mathcal{P}$ it does not mean that orientations described by W of $\mathcal{P}$ and by W^+ of $\mathcal{H}_\mathcal{S}$ are identical. They can be mirror-symmetric again, so that orientation descriptions related to $\mathcal{P}$ and to $\mathcal{S}$ will not be congruent.

3.2.3. Encoding for neither centrosymmetric nor enantiomorphic point groups.

Finally, we consider the case that a group is not centrosymmetric but contains improper rotations. We also presuppose a point-group sensitive indexing procedure as demonstrated in (Winkelmann & Nolze, 2015*b*) using a suitable automated indexing of standard EBSD patterns of $\mathrm{A^{III}B^V}$ semiconductors ($\mathcal{P} = \bar{4}3m$).

Based on a Hough-transformation related orientation determination using the respective Laue symmetry $\mathcal{S} = m\bar{3}m$, the derived orientation descriptions are first related to the enantiomorphic subgroup $\mathcal{H}_\mathcal{S} = 432$, which is presently standard for all existing measuring systems.

The point-group sensitive orientation evaluation is performed in a post-processing of pattern and orientation data. Since $\bar{4}3m$ does not contain any 90° rotation operation around $\langle 0\,0\,1 \rangle$, subsequently the two possible pseudo-solutions (ϕ_1, Φ, ϕ_2) and ($\phi_1, \Phi, \phi_2 + 90°$) will be evaluated. This happens by pattern matching of the experimental Kikuchi signal with in real-time derived pattern simulations (Winkelmann *et al.*, 2007), and including an orientation refinement. A better image correlation finally indicates the correct solution.

Since the orientation description is now based on the point group $\mathcal{P} = \bar{4}3m$, all Euler angles are related to the maximal enantiomorphic subgroup $\mathcal{H}_\mathcal{P} = 23$. Exemplarily, in Fig. 13

Laue-group specific as well as point-group specific orientation data of a polycrystalline microstructure of GaP are compared using the color keys of the respective enantiomorphic subgroups $\mathcal{H}_\mathcal{S} = 432$ (a) and $\mathcal{H}_\mathcal{P} = 23$ (b). The respective color keys are given in Fig. 14 (a+b).

a)

b)
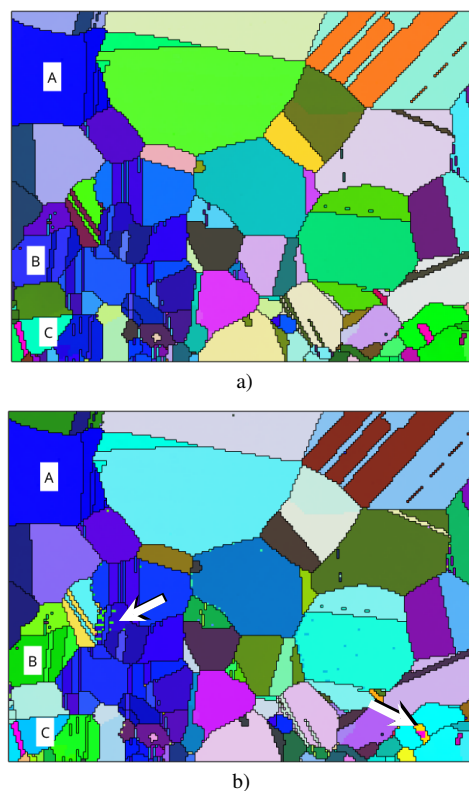
Figure 13
IPF map of a polycrystalline GaP microstructure indexed according to the Laue groups $m\bar{3}m$ (a), or to the point group $\bar{4}3m$ (b). The applied color keys are based on the enantiomorphic symmetry group 432 (a) or on 23 (b), cf. Fig. 14.

In both IPF-encoded orientation maps A, B, and C indicate three independent grains. Although the first map suggests that A and B are similarly aligned, while C is differently oriented, the computation of the misorientation angles $\Delta\varphi$ gives for grains A and B $\Delta\varphi = 78°$, between B and C $\Delta\varphi = 60°$, and for grains A and C results $\Delta\varphi = 26°$. These values are much better represented by the color-encoding in (b).

The reason for the color differences of *h* are mainly controlled by the selected group symmetry. The multiplicities of 48 (for $\mathcal{S} = m\bar{3}m$), 24 (for $\mathcal{P} = \bar{4}3m$ but also $\mathcal{H}_\mathcal{S} = 432$), and 12 (for $\mathcal{H}_\mathcal{P} = 23$) indicate that with respect to the point group $\mathcal{P}$ the size of the fundamental sector has to be twice bigger for $\mathcal{H}_\mathcal{P}$, twice smaller for $\mathcal{S}$, and identical for $\mathcal{H}_\mathcal{S}$. In order to make a comparison easier, in Fig. 14 an identical spherical segment is displayed which represents the fundamental sector of $\mathcal{H}_\mathcal{P}$ but consists, e.g., for $\mathcal{S}$ of four fundamental sectors.
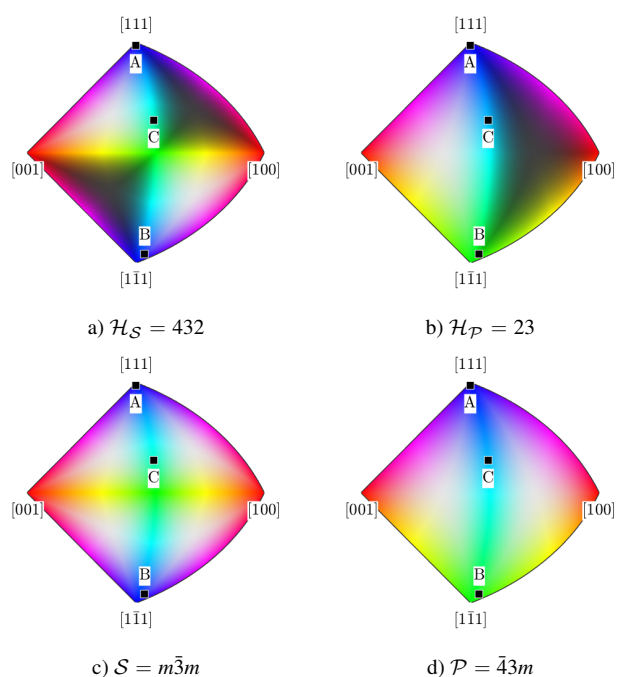
Figure 14
IPF keys for 432, 23, the centrosymmetric point groups $m\bar{3}m$ and $\bar{4}3m$ with the mean orientations of the grains A, B, and C annotated. For 432 and $\bar{4}3m$ the fundamental sector has been doubled and for $m\bar{3}m$ has been quadrupled to cover the same sector as for 23.

As already illustrated at the example of quartz, any transition to a higher-symmetric description is connected to some kind of loss of information which cannot get back. Whereas [1 1 1] and [1 $\bar{1}$ 1] with respect of $\mathcal{P} = \bar{4}3m$ are independent, the indexing according to $\mathcal{S} = m\bar{3}m$ does not enable anymore to distinguish between them. Also the orientation description with respect to $\mathcal{H}_\mathcal{S} = 432$ distinguishes mathematically between h and $-h$, but not physically. A respective color mapping will not be able to express the polarity of [1 1 1] and [1 $\bar{1}$ 1], cf. Fig. 13 (a). In contrast, a transition to the lower-symmetric $\mathcal{H}_\mathcal{P} = 23$ keeps the capability to distinguish between [1 1 1] and [1 $\bar{1}$ 1] (Fig. 13 (b)), and it is also able to separate between mirror-symmetric orientations.

In summary, for this most general case four possible IPF-color keys are available. The use of $\mathcal{P}$ and $\mathcal{S}$ enables a crystallographic evaluation of a reference direction r as symmetry-equivalent h, where $\mathcal{S}$ equalizes reverse directions which are perhaps required to distinguish polar properties. The application of the color-keys of the enantiomorphic groups $\mathcal{H}$ is more suitable for a reliable visualization of crystal orientation data.

3.3. The agony of choice: Appropriate color key selection

IPF-coloring is more diverse than commonly assumed, and the currently applied coloring represents only one opportunity with a limited validity. The previous discussion demonstrated that a meaningful coloring and a correct IPF key selection finally depends on the aim of visualization. Consistent for all IPF-encodings is, that any orientation **G** is reduced to a description of a single reference direction r as crystallographically symmetry-equivalent $\boldsymbol{W}^{-1}h$. It requires a critical analysis by the operator which group symmetry will be able to represent the extracted orientation information in a best or at least meaningful way. If the aim of the typically only qualitative demand is an easily visible correlation between a single reference direction r and an observable anisotropic alignment of crystals, the simplified use of $\mathcal{P}$ or even $\mathcal{S}$ is expedient. However, for a more orientation related representation $\mathcal{H}_\mathcal{P}$ or even $\mathcal{H}_\mathcal{S}$ are the better choice.

The currently exclusively available IPF coloring using the Laue group $\mathcal{S}$ is only meaningful, if the crystal structure is centrosymmetric ($\mathcal{P} = \mathcal{S}$), or an indexing with respect to the not centrosymmetric signal is impossible or of low reliability (pseudo-symmetry). There are alternative imaging tools available in software packages like different kinds of misorientation mappings, but they do not map the orientation itself. The here suggested IPF coloring using the fundamental sector of the enantiomorphic subgroup of $\mathcal{P}$ represents a very straightforward tool. It perfectly matches the practically omnipotent orientation description by Euler angles without having their disadvantage of generating discontinuities during Euler space coloring. Furthermore, enantiomorphic groups represent the only set of symmetries which do not generate any color jumps in grains if the here suggested color distributions are used.

A new imaging opportunity but also gain in information is related to the case that the structure of a phase is not centrosymmetric, and the Kikuchi signal allows a differentiation between opposite directions h and $-h$, cf. the example of GaP. Every analytical system here which postulates the validity of Friedel's law for EBSD is *a priori* lost. Even in case one would own a dataset containing point-group sensitive orientation descriptions, they can only be processed by making them centrosymmetric first. Because of the discriminability between h and $-h$, point-group related IPF keys enable to distinguish between polar direction in crystals, and because of their definition between non-polar directions also (Nolze *et al.*, 1990). Wherever the unacceptable symmetrization to the Laue symmetry limits an interpretation of observed phenomena the point-group symmetry related interpretation of orientation data might be essential.

Nevertheless, as for the Laue-group related imaging the application of the IPF key of the point group only describes the impact of **G** on r and not of **G** itself. In order to get a unique impression about **G** the respective enantiomorphic group of $\mathcal{P}$ needs to be used. Then also the impact of **G** on r is visualized, but at least all h which are not connected by any proper crystallographic rotation are colored differently, even if they are crystallographically equivalent.

4. Summary and conclusions

Current IPF coloring is strongly limited. The presently offered fundamentals sectors are for some reasons incomplete (only one axes setting available for each group, or keys are missing for low symmetries), and limited on the 11 Laue groups. Moreover, for 7 from 11 Laue groups the presently used standard color distribution generates discontinuities within grains which is misinterpretable as orientation errors. In general, the limitation on Laue groups is unreasonable since EBSD is a technique

which does not fulfill Friedel's rule. To overcome all of these problems a complete set of color keys has been derived which do not generate exaggerated color jumps and produce a homogeneous color variation even in case of a continuous change of orientation. This is demonstrated on the example of quartz.

It has been shown that only for $\bar{1}$, $\bar{3}$ and $\bar{4}$ a definition of color keys without the ability to generate color jumps in single grains is impossible. For $\bar{1}$ a possible solution is given which permits a color assignment not only to one non-symmetry-equivalent direction.

The difference between an IPF-coloring of symmetry-equivalent reference directions using point or Laue group, and of reference directions which originate from really symmetry-equivalent orientations using enantiomorphic (rotational) groups has been discussed.

At the example of a high-symmetric cubic transformation structure it has been demonstrated that in contrast to the common opinion even the combination of several IPF-colorized maps are typically not suitable to display orientations unequivocally.

The color distribution within the keys, cf. e.g.; (Schwarzer & Sukkau, 2013; Nolze, 2013; Kayser, 2010), but sometimes also the shape of the fundamental sectors varies from definition to definition. Therefore, for a general interpretation of colorized IPF maps a standardization of size, shape and color distribution would be reasonable. The paper suggests a more regular distribution of colors in order to recognize orientation variations not only for specific colors. All color keys are implemented in the Matlab toolbox MTEX 4.3. Commented scripts that generate all figures but Fig. 2 of the paper can be found at http://mtex-toolbox.github.io/publications.html.

References

Baba-Kishi, K. Z. (1991). *J. Appl. Cryst.* **24**(2), 38–47.

Bachmann, F., Hielscher, R. & Schaeben, H. (2010). *Sol. State Phenom.* **160**, 63–68.

Bunge, H. (1982). *Texture Analysis in Materials Science: Mathematical Methods.* London: Butterworths,London ; Boston.

Hahn, T. (ed.) (1995). *International Tables for Crystallography*, vol. A: Space-Group Symmetry. Kluver Academic Publishers, Dordrecht, Boston, London, 4th ed.

Inokuti, Y., Maeda, C. & Ito, Y. (1987). *Trans. ISIJ*, **27**, 302–311.

Kayser, T. (2010). *Characterization of microstructure in aluminum alloys based on electron backscatter diffraction.* Ph.D. thesis, TU Dortmund, Germany.

Kocks, U., Tomé, C. & Wenk, H. (1998). *Texture and Anisotropy: Preferred Orientations in Polycrystals and their Effect on Materials Properties.* Cambridge: Cambridge University Press.

Massey, W. S. (1959). *Pacific J. Math.* **9**(3), 783–789.

Nolze, G. (2013). *Cryst. Res. Technol.* **48**(7), 476–489.

Nolze, G. (2015). *Cryst. Res. Technol.* **50**(2), 188–201.

Nolze, G., Geist, V., Wagner, G., Paufler, P. & Jurkschat, K. (1990). *Z. Kristallogr.* **193**(1-2), 111–126.

Nolze, G., Grosse, C. & Winkelmann, A. (2015). *J. Appl. Cryst.* **48**, 1405–1419.

Nolze, G., Winkelmann, A. & Boyle, A. P. (2016). *Ultramicroscopy*, **160**(1), 146–154.

Patala, S., Mason, J. K. & Schuh, C. A. (2012). *Progr. Mater. Sci.* **57**, 1383–1425.

Patala, S. & Schuh, C. A. (2011). *Acta Mater.* **59**, 554–562.

Randle, V. & Engler, O. (2000). *Introduction to Texture Analysis: Macrotexture, Microtexture & Orientation Mapping.* Singapore: Gordon and Breach Science Publishers.

Schwartz, A. J., Kumar, M. & Adams, B. L. (eds.) (2000). *Electron Backscatter Diffraction in Materials Science*. Netherlands: Kluver Academic/Plenum Publishers, New York, Boston, Dordrech, London, Moscow, 1st ed.

Schwartz, A. J., Kumar, M., Adams, B. L. & Field, D. P. (eds.) (2009). *Electron Backscatter Diffraction in Materials Science*. Springer Science+Business Media.

Schwarzer, R. & Sukkau, J. (2013). *Banaras Metall.* **18**, 1–12.

Winkelmann, A. & Nolze, G. (2015a). *Ultramicroscopy*, **149**(2), 58–63.

Winkelmann, A. & Nolze, G. (2015b). *Appl. Phys. Lett.* **106**, 072101.

Winkelmann, A., Trager-Cowan, C., Sweeney, F., Day, A. & Parbrook, P. (2007). *Ultramicroscopy*, **107**(4-5), 414–421.

Appendix A
Color definition in color keys

This section covers the technical details in the definition of the HSV color values as described in Sections 2.2 and 2.4.

A.1. An adapted hue gradient

This section covers the technical details in the definition of the HSV color values as described in Sections 2.2 and 2.4. One issue is that for linear hue the colors are unevenly distributed, see Figure 16a. For this reason we do not go with constant speed through the hue but define a speed function $v(\rho)$ which is larger around the colors red, blue and green,

$$v(\rho) = 0.5 + e^{-\frac{4}{7}\rho} + e^{-\frac{4}{7}[\rho-120]} + e^{-\frac{4}{7}[\rho+120]}$$

where $[\rho]$ is the projection of the angle ρ into the interval $[-180°, 180°]$. The hue $h(\omega)$ as function of the angle ω is now defined as

$$h = \int_0^\omega v(\rho)\,\mathrm{d}\rho. \tag{5}$$

(a) linear hue gradient

(b) customized hue gradient

Figure 15
Linear and customized hue gradient

A second issue is that in spherical triangles the distance $d(\rho)$ between the barycenter and the boundary might vary significantly with the angle ρ. As a consequence colors associated with directions that correspond to long distances, e.g.,towards the vertices of the triangle, cover a larger area then colors associated with directions that correspond to small distances. In order to distribute the colors more uniformly we set the speed

function $v(\rho)$, which we use for re-scaling the hue, proportional to distance to the boundary $d(\rho)$, i.e.,

$$v(\rho) = d(\rho) \left(0.5 + e^{-\frac{4}{7}\rho} + e^{-\frac{4}{7}[\rho - 120]} + e^{-\frac{4}{7}[\rho + 120]} \right).$$

Finally, we would like to have the three corners of a triangle to be associated with the colors red, green and blue. However, for extremely acute-angled triangles the angles ω_1, ω_2, ω_3 between the barycenter and the three corners may be very differently. To compensate for this we normalize the speed function $v(\rho)$ such that

$$\int_0^{\omega_1} v(\rho)d\rho = \int_{\omega_1}^{\omega_1 + \omega_2} v(\rho)d\rho = \int_{\omega_1 + \omega_2}^{360} v(\rho)d\rho = 1/3.$$

A.2. An adapted lightning and saturation gradient

The use of a linear map between the polar angle ρ and the lightning L has the effect that the white region in the IPF key is rather small when compared to the red, green or blue regions, cf. Fig. 1(d) or Fig. 16(a). In this paper we used the following map for a more balanced key

$$L = \lambda_L \frac{\rho}{\pi} + (1 - \lambda_L) \sin^2 \frac{\rho}{2},$$

where the first summand is the linear map and the second summand is a map with a steeper gradient close to the poles. The parameter λ_L allows to fine-tune between a small and a large white spot in the center. For $\lambda_L = 1$ we obtain the common linear map whereas $\lambda_L = \frac{1}{4}$ gives a more balanced key, cf. 16(b).

Using all saturated colors, and in particular, black and white for the colorization of orientations has the disadvantage that there is no color left that sticks out and can be used for annotations, drawing grain boundaries, marking not indexed pixels. A possible workaround is not to use black and white for the center of the spherical triangles but bright and dark gray. This can be achieved by setting this saturation S as a function of the lighting L,

$$S = 1 - 2\lambda_S |L - 0.5|.$$

Here, the parameter λ_S controls how grayish the center are colored. For $\lambda_S = 0$ we keep white and black center, while $\lambda_S = 1$ results in bright gray and dark gray being identical. A good balance seems to be $\lambda_S = 0.25$ which was used in Fig. 16(c).

(a) $\lambda_L = 1$, $\lambda_S = 0$ (b) $\lambda_L = 0.2$, $\lambda_S = 0$ (c) $\lambda_L = 0.2$, $\lambda_S = 0.2$
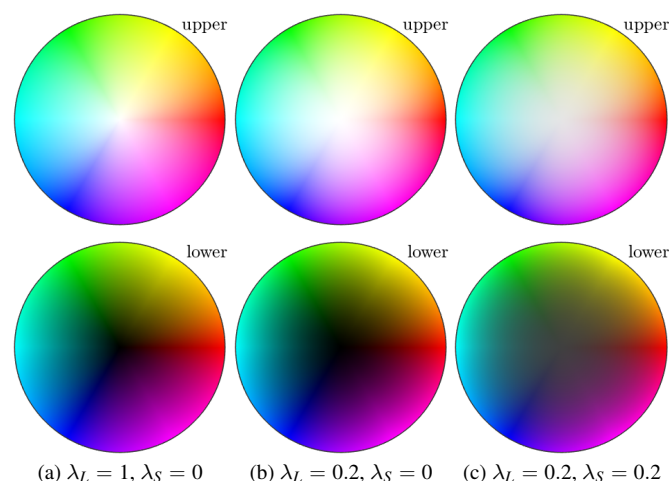
Figure 16
Triclinic IPF key with different scalings for lightning L and saturation S. The common linear scale is visualized in (a), while (b) displays a non linear lightning scaling and (c) displays non linear lightning in combination with lightning dependent saturation.

Appendix B
A complete list of color keys

The color distributions are displayed as equal area projections.

4

4/*m*

4*mm*

422

$\bar{4}2m$

$\bar{4}m2$

4/*mmm*